the activation energy barrier for the transformation to massicot

Thus it may be seen that the measurement of microstrains can throw considerable light on the way that the energy required to mount the activation energy barrier is produced in the lattice, and also on the effect of shear forces on pressure–temperature phase diagrams.

References

APPELT, K., ELBANOWSKI, M. & NOWACKI, A. (1962). *Electrochem. Acta*, **6**, 207.

AVRAMI, M. (1939). *J. Chem. Phys.* **7**, 1103.

AVRAMI, M. (1940). *J. Chem. Phys.* **8**, 212.

AVRAMI, M. (1941). *J. Chem. Phys.* **9**, 177.

BERTAUT, E. F. (1952). *Acta Cryst.* **5**, 117.

CLARK, G. L. & ROWAN, R. (1941). *J. Amer. Chem. Soc.* **63**, 1302.

DACHILLE, F. & ROY, R. (1960). *Nature, Lond.* **186**, 34.

DACHILLE, F. & ROY, R. (1961). In *Reactivity of Solids*. Edited by DEBOER, J. H. *et al.* p. 502. New York: Elsevier Publishing Co.

DICKENS, B. (1965*a*). *J. Inorg. Nucl. Chem.* **27**, 1495.

DICKENS, B. (1965*b*). *J. Inorg. Nucl. Chem.* **27**, 1503.

KUMAZAWA, M. (1963). *J. Earth Sci. Nagoya Univ.* **11**, 145.

LANGFORD, J. I. & WILSON, A. J. C. (1963). In *Crystallography and Crystal Perfection*. Edited by RAMACHANDRAN, G. N. p. 207. London: Academic Press.

LAUE, M. VON (1926). *Z. Kristallogr.* **64**, 115.

LEWIS, D. & LINDLEY, M. W. (1966). *J. Amer. Ceram. Soc.* **49**, 49.

LEWIS, D. & NORTHWOOD, D. O. (1968). *Strain*, **4**, 19.

LEWIS, D. & NORTHWOOD, D. O. (1969). *Brit. J. Appl. Phys. (J. Phys. D.)*. **2**, 21.

MOORE, W. J. & PAULING, L. (1941). *J. Amer. Chem. Soc.* **63**, 1392.

NORTHWOOD, D. O. (1968). Ph. D. Thesis, Univ. of Surrey.

PORTER, L. J. (1968). Private communication.

RICHARDS, B. P. & GREENHAM, A. C. (1968). *Brit. J. Appl. Phys. (J. Phys. D.)*. **1**, 1297.

WARREN, B. E. & AVERBACH, B. L. (1950). *J. Appl. Phys.* **21**, 595.

WHITE, W. B., DACHILLE, F. & ROY, R. (1961). *J. Amer. Ceram. Soc.* **44**, 170.

WILSON, A. J. C. (1962). *Proc. Phys. Soc. (London)*. **80**, 286.

ZAKI, H. M. (1967). Private communication.

J. Appl. Cryst. (1969). **2**, 164

The Structure of Vitreous Silica*

BY R. L. MOZZI† AND B. E. WARREN

Research Laboratory of Electronics, Massachusetts Institute of Technology, Cambridge, Massachusetts U.S.A.

(*Received* 24 *February* 1969)

A new study of the structure of vitreous silica has been made under greatly improved conditions. Using Rh $K\alpha$ radiation with the method of fluorescence excitation, reliable intensity values were measured to $4\pi \sin\theta/\lambda = 20$. The interpretation was in terms of pair functions, thereby eliminating the approximations in earlier work. Each silicon is tetrahedrally surrounded by 4 oxygen atoms, with a Si–O distance which is closely 1·62 Å. Each oxygen atom is bonded to 2 silicon atoms. The Si–O–Si bond angle α shows a distribution $V(\alpha)$ extending all the way from 120° to 180°, with a maximum at $\alpha = 144°$. This wide variation in α is an important distinction between the vitreous and the crystalline forms of silica, and it furnishes an important criterion for any proposed model of vitreous silica. Good agreement with the measured pair function distribution curve was obtained by assuming a random orientation about the Si–O bond directions. The interpretation leads to the familiar random network model, but with the new results the model is more precise.

Introduction

The structure of vitreous silica has been the subject of several earlier X-ray diffraction and neutron diffraction studies (Warren, Krutter & Morningstar, 1936; Valenkov & Porai-Koshitz, 1936; Zarzycki, 1957; Carraro & Domenici, 1963; Henninger, Buschert & Heaton, 1967). In the early X-ray studies there were severe experimental and theoretical difficulties which limited considerably the possibility of obtaining results of the desired accuracy. The most serious of these difficulties have now been overcome, so that it is well worthwhile to restudy the structures of simple glasses such as vitreous silica.

To obtain high resolution in the final distribution curve, it is necessary to have very accurate intensity measurements out to the largest possible values of $\sin\theta/\lambda$. For this purpose it is desirable to use a short wave length radiation. But for materials of low atomic number such as SiO_2, the Compton modified intensity is as much as four or five times the intensity of unmodified scattering at the high $\sin\theta/\lambda$ values that are

* This work was supported principally by the Joint Services Electronics Program (Contract DA 28-043-AMC-02536 E).

† Present address: Research Division, Raytheon Co., Waltham, Massachusetts 02154, U.S.A.

of interest. With the unmodified intensity buried under a Compton scattering four or five times as large, it is quite impossible to obtain accurate values, and this has been one of the major experimental difficulties. Obviously it is necessary to eliminate the Compton scattering in the measuring process.

This can be done conveniently by using the method of fluorescence excitation (Warren & Mavel, 1965). A primary beam consisting of crystal monochromated Rh $K\alpha$ radiation falls upon the sample. The scattered radiation, comprising both the unmodified and the modified components, enters the receiving slit and falls upon a sheet of Mo at 45° to the beam. The Mo fluorescence K radiation, which is excited, is received by a krypton filled counter at 90° to the diffracted beam and close to the Mo foil. Since λ (Rh $K\alpha$)= 0·615 Å and λ (Mo, K edge)=0·620 Å, most of the Compton scattering is of too long a wavelength to be able to excite fluorescence radiation, and what we measure is largely due to the unmodified scattering. The efficiency of this process is about 0·5%, which means that for 200 unmodified quanta entering the receiving slit, one count will be recorded in the krypton counter. The efficiency is high enough, and by this method it is now possible largely to eliminate the strong Compton scattering at high values of $\sin\theta/\lambda$.

In the early X-ray studies, the interpretation was based upon the approximation that the different atomic scattering factors f could be considered as proportional to one another. In general this is a rather rough approximation. For materials containing more than one kind of atom, the present method of interpretation is based upon the use of pair functions, a concept first developed in the Norwegian school of C. Finbak. A rigorous treatment using the pair function has been published (Warren, 1969).

It is convenient to introduce the term unit of composition (uc), where for vitreous silica, the obvious unit would be 1 silicon and 2 oxygen atoms. The kinds of atoms in the unit of composition are denoted by the index j. We now summarize the necessary relations.

$$i(k)=\frac{I_{eu}/N-\sum_{uc} f_j^2}{g^2(k)} \tag{1}$$

$$P_{ij}(r)=\int_0^{k_m}\frac{f_i f_j}{g^2(k)}\,e^{-\alpha^2k^2}\sin kr_{ij}\sin krdk \tag{2}$$

$$Q_{ij}(x)=\frac{1}{2}\int_0^{k_m}\frac{f_i f_j}{g^2(k)}\,e^{-\alpha^2k^2}\cos xkdk \tag{3}$$

$$P_{ij}(r)=Q_{ij}(r-r_{ij})-Q_{ij}(r+r_{ij}) \tag{4}$$

$$A_{ij}=\int P_{ij}(r)dr=(\pi/2)Z_iZ_j \tag{5}$$

$$\sum_{uc}\sum_{i}\frac{N_{ij}}{r_{ij}}P_{ij}(r)=2\pi^2r\varrho_e\sum_{uc}Z_j+\int_0^{k_m}ki(k)e^{-\alpha^2k^2}\sin rkdk \tag{6}$$

where

$$k=4\pi\sin\theta/\lambda\,.$$

I_{eu}/N is the intensity of unmodified scattering in electron units per unit of composition.

$g(k)$ is a sharpening factor which decreases with k, it is chosen to be approximately unity at $k=0$. In this study we use for $g(k)$ the scattering factor per electron $f_e=\sum_{uc} f_j/\sum_{uc} Z_j$. Because of the dispersion terms, $g^2(0)=f_e(0)f_e^*(0)$ is a little greater than unity at $k=0$.

r_{ij} is the distance from an atom j to an atom in the ith shell of surrounding atoms.

$P_{ij}(r)$ is the pair function for two atoms i and j.

k_m is the cut off value of k, the maximum value to which it was possible to make measurements.

$\exp[-\alpha^2k^2]$ is a convergence factor, introduced to minimize termination satellites, and weight down the inaccurate measurements at high values of k.

$Q_{ij}(x)$ is an auxiliary function which is readily calculated, and in terms of which $P_{ij}(r)$ is conveniently expressed. In equation (4), the second term $Q_{ij}(r+r_{ij})$ is usually negligible.

A_{ij} is the area under the $P_{ij}(r)$ pair function curve.

Z_j is the number of electrons in the atom or ion.

N_{ij} is the number of neighbors in the ith shell about an atom j.

ϱ_e is the average electron density.

In equation (6) the first term on the right is evaluated from the density and composition of the sample. The second term on the right is evaluated for a series of values of r using the experimental intensity curve I_{eu}/N, the experimental cut off value k_m, a convergence coefficient α chosen for convenience, and a sharpening factor $g(k)$ which in this case was taken as f_e. The quantity on the left of equation (6) is called the pair function distribution (P.F.D.). The sum of the two quantities on the right gives an experimentally measured pair function distribution curve. Interatomic distances are given by the positions of the peaks in the experimental curve. The number of neighbors is obtained by finding the numbers N_{ij} which must be used to make the calculated P.F.D. on the left of equation (6) match the measured curve obtained from the right hand side. The treatment is rigorous and completely free from approximations, because whatever values of k_m, α and $g(k)$ are used on the right hand side of equation (6), the same values are used in evaluating the pair functions by means of equation (3).

For vitreous SiO_2 there are three combinations to consider: Si–O, O–O and Si–Si. Using tabulated values of the atomic scattering factors and dispersion corrections (Cromer & Waber, 1965; Cromer, 1965) and with $k_m=21{\cdot}1$, $\alpha=0{\cdot}056$ and $g(k)=f_e$, the three pair functions $Q_{ij}(x)=P_{ij}(r-r_{ij})$ were evaluated by means of equation (3). The curves are shown on Fig. 1. Each pair function is symmetrical about $x=0$ and peaks at $x=r-r_{ij}=0$. The ripples represent the termination satellites, in general they cause no harm since exactly the same ripples will be present in the experimental

curve. In addition to the central peak, there are pronounced wings, which on the average are positive for O–O and negative for Si–Si.

Experimental

The sample of vitreous silica was a plate 4·0 × 4·0 × 0·3 cm cut from optical quality fused quartz supplied by Engelhard Industries Inc. under the trade name Amersil. The measured density was 2·20 g.cm^{-3}. The experimental intensity curve was obtained by combining measurements made with Cu $K\alpha$ ($\lambda = 1{\cdot}542$ Å) and Rh $K\alpha$ ($\lambda = 0{\cdot}6147$ Å).

For the measurements with Cu $K\alpha$, a bent and ground LiF crystal diffracted monochromatic Cu $K\alpha$ to an entrance slit. The entrance slit and the receiving slit were each 14 cm from the sample. The diffracted intensity entered an argon filled counter situated immediately behind the receiving slit, and the intensities were registered by a chart recorder. A correction was made for air scattering, which was found to be negligible except at small angles. The chart recording included both the unmodified and the Compton modified intensities. The curve was divided by a polarization factor, and normalized to electron units per unit of composition by a modification of the Norman method (Norman, 1957). After making a small correction for multiple scattering (Warren & Mozzi, 1966), the modified component was subtracted using tabulated values of the modified intensity per atom (*International Tables for X-ray Crystallography*, 1962). Using Cu $K\alpha$ it is not too bad to include both the unmodified and the modified components in the measured intensity, since at the worst the modified intensity is about one third of the total for silica. The measurements with Cu $K\alpha$ covered the range $k = 0{\cdot}0$ to $k = 7{\cdot}5$.

The measurements with Rh $K\alpha$ covered the range $k = 7{\cdot}0$ to $k = 20{\cdot}0$, and the Compton scattering was largely eliminated by the method of fluorescence excitation. Between $k = 7$ and $k = 12$, there was a small contribution by Compton scattering owing to the fact that in this angular range a non-negligible fraction of the modified scattering is of wavelength less than λ (Mo, K edge). A correction was made by measuring at several values of k the fraction of modified scattering of wavelength less than λ (Mo, K edge) = 0·620 Å. The correction for air scattering was found to be negligible. Dividing by the appropriate polarization factor, the curve was changed to absolute units by choosing a

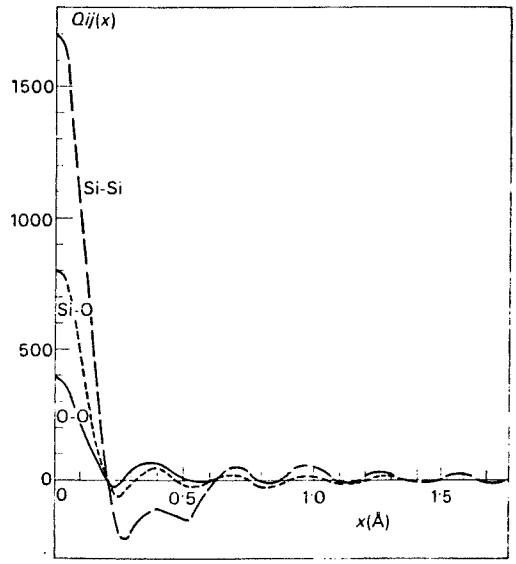

Fig. 1. Computed pair functions for SiO_2, with $\alpha = 0{\cdot}05$, $k_m = 21{\cdot}1$, and $g(k) = f_e$.

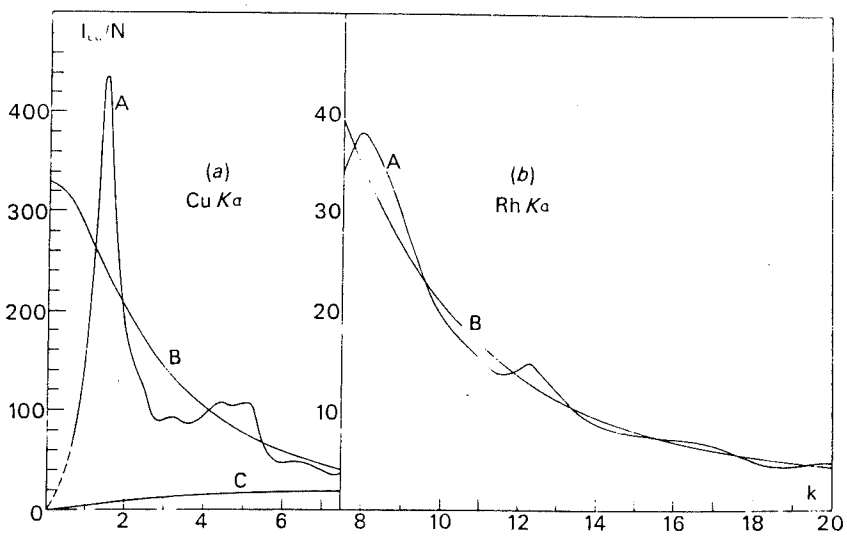

Fig. 2. Measured intensity curves for SiO_2, (*a*) with Cu $K\alpha$, (*b*) with Rh $K\alpha$. Curve *A*, the unmodified intensity I_{eu}/N. Curve *B*, the independent unmodified intensity Σf_j^2. Curve *C*, the Compton modified intensity which had been subtracted.

uc

factor for the ordinate scale, such that at high k, the curve oscillated positive and negative about the independent unmodified curve $\Sigma_{uc} f_i^2$. A correction was made for multiple scattering. A detailed description of the methods used for making the various experimental corrections will be presented in a separate contribution.

The intensity curves I_{eu}/N in electron units per unit of composition which were obtained from the Cu $K\alpha$ and Rh $K\alpha$ measurements are shown by Fig. 2. Combining the two curves and using $g(k)=f_e$, we obtain the function $ki(k)$. Adding a convergence factor with a coefficient $\alpha=0{\cdot}056$, produces the curve $ki(k)\exp[-\alpha^2k^2]$ which is shown by Fig. 3. The right hand side of equation (6) was then evaluated for a series of values of r, and the resulting pair function distribution curve is shown by Fig. 4. In general there will be small errors in the experimental curve. If in the $ki(k)\exp[-\alpha^2k^2]$ curve there is a small excess $\delta(k)$ in the vicinity of $k=k_o$, it follows from equation (6) that there will be a corresponding error $\Delta(r)$ in the measured distribution curve

$$\Delta(r)=[\int \delta(k)\mathrm{d}k]\sin k_o r\,.$$

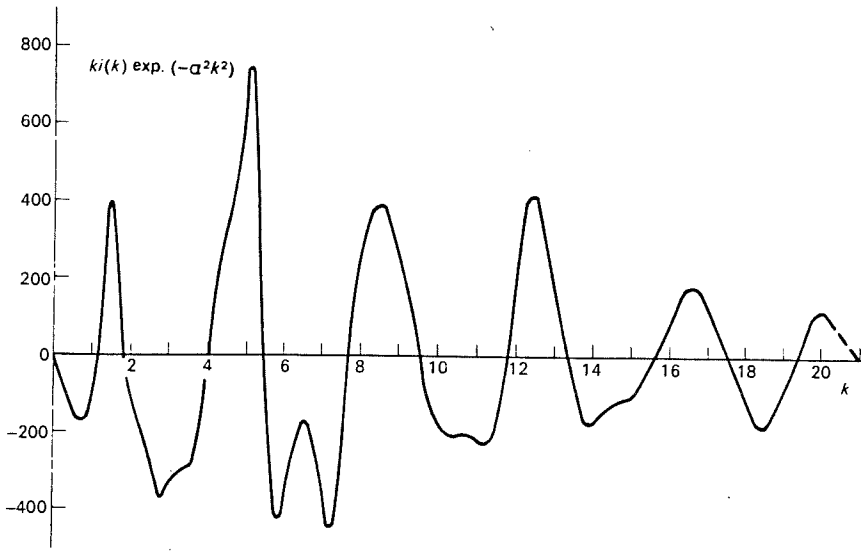

Fig. 3. The experimental $ki(k)\exp(-\alpha^2k^2)$ for SiO_2, with $\alpha=0{\cdot}056$ and $g(k)=f_e$.

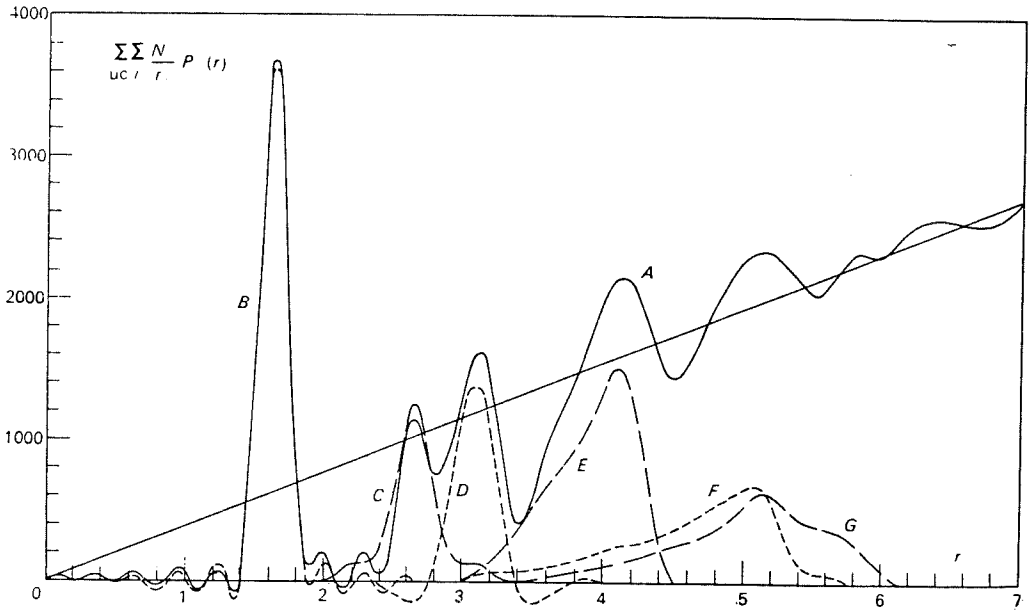

Fig. 4. The pair function distribution curves for SiO_2. *A* is the measured curve. The computed contributions are given by: *B*, Si–O; *C*, O–O; *D*, Si–Si; *E*, Si–2nd O; *F*, O–2nd O; *G*, Si–2nd Si.

The error is sinusoidal in r, and most easily recognized in the small r region between $r=0$ and the first peak. Since the error is sinusoidal, it does not change the total area if k_o is not too small. The measured pair function distribution curve, which was first obtained, showed such a sinusoidal error term of the form $-100 \sin 5{\cdot}2r$, and the curve of Fig. 4 has been corrected by this amount.

Interpretation

In crystalline silicates, each silicon atom is tetrahedrally surrounded by 4 oxygen atoms with a Si–O distance of about 1·62 Å, and an O–O distance of about 2·65 Å. With this information, the first peak on the distribution curve of Fig. 4, occurring at $r=1{\cdot}62$ Å, is readily identified as a Si–O peak. Similarly the second peak at $r=2{\cdot}65$ Å can be identified as an O–O peak. The ratio of the two distances $2{\cdot}65/1{\cdot}62=\sqrt{8/3}$ is exactly what would be expected for tetrahedral bonding

In principle the number of neighbors about an atom can be obtained by comparing the peak area on the experimental curve to the area of the pair function as given by equation (5). In practice, however, there are serious difficulties in this direct approach. There are wings on the pair functions and corresponding wings on the experimental peaks, and except for the first peak, there is serious overlapping of the peaks. It is better to find by trial the values of N_{ij} and the distributions of r_{ij} which must be assumed to bring the sum of the computed pair functions into agreement with the experimental curve of Fig. 4.

We start by assuming that each silicon is bonded to 4 oxygen atoms, and each oxygen is bonded to 2 silicon atoms. The first peak is due to oxygen atoms about a silicon and silicon atoms about an oxygen atom, and in the unit of composition there are 1 silicon and 2 oxygen atoms. For the first peak

$$\sum_{\text{uc}} \sum_{i} N_{ij}/r_{ij}=(1\times 4+2\times 2)/1{\cdot}62=8/1{\cdot}62\,.$$

If the computed silicon–oxygen pair function $P_{ij}(r)$ is multiplied by 8/1·62 and plotted on the first peak of Fig. 4, it is found that the areas of the two peaks are closely the same, but that the measured peak is a little lower and broader than the computed peak. This indicates that there is a small variation in the silicon–oxygen distance about the mean value 1·62 Å. Part of this variation is, of course, due to temperature vibration. To represent the variation in neighbor distance, we introduce a distance distribution function $G(r_{ij})$. The effective pair function $P'_{ij}(r)$ is then given by a convolution with $G(r_{ij})$.

$$P'_{ij}(r)=\int G(r_{ij})Q(r-r_{ij})dr_{ij}\,. \qquad (7)$$

In principle $G(r_{ij})$ could be obtained by a deconvolution of the terms in equation (7), but since the variation in distance is small, it is better to use trial functions $G(r_{ij})$. The selected function will, of course, be far from unique, but it will represent the magnitude of the distance variation. A satisfactory fit was obtained by using for $G(r_{ij})$ values proportional to 1·00 for $r_{ij}=1{\cdot}62$, 0·50 for $r_{ij}=1{\cdot}62\pm 0{\cdot}05$, and 0·15 for $r_{ij}=1{\cdot}62\pm 0{\cdot}10$. The calculated pair function distribution curve for silicon–oxygen neighbors is represented on Fig. 4 by the dashed curve centered at $r=1{\cdot}62$ Å. There is satisfactory agreement for both the main peak and the termination satellite ripples.

There are 2 oxygen atoms in the unit of composition and each oxygen should have 6 nearest oxygen neighbors, so that for the oxygen–oxygen peak

$$\sum_{\text{uc}} \sum_{i} N_{ij}/r_{ij}=2\times 6/2{\cdot}65\,.$$

In this case there is a larger distance variation, and a satisfactory $G(r_{ij})$ was obtained by using values proportional to 1·00 for $r_{ij}=2{\cdot}65$, 1·00 for $r_{ij}=2{\cdot}65\pm 0{\cdot}05$, 1·00 for $r_{ij}=2{\cdot}65\pm 0{\cdot}10$ and 0·50 for $r_{ij}=2{\cdot}65\pm 0{\cdot}15$. The calculated pair function distribution curve for oxygen–oxygen neighbors is shown on Fig. 4 by the dashed curve centered at $r=2{\cdot}65$ Å. Beginning with

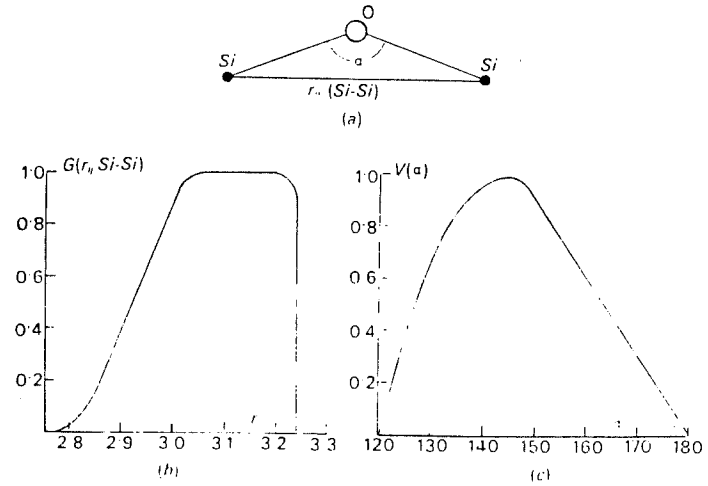

Fig. 5. The Si–O–Si bond angle α. (*a*) The relation between α and the Si–Si distance. (*b*) the distribution function $G(r_{ij})$ for the Si–Si distance. (*c*) the distribution function $V(\alpha)$.

ak, it is no longer possible to judge the quality of fit, peak by peak, because of the strong overlapping peaks. It is necessary to wait until several peaks have en calculated and then compare the sum of the calated peaks with the measured distribution curve. The third peak on Fig.4 is at $r=3{\cdot}12$ Å and this is a con–silicon contribution. Since $3{\cdot}12<2\times1{\cdot}62$, it is dent that the Si–O–Si bond angle α is less than 180°, d that there is an appreciable variation in this angle ce the third peak is much broader than the Si–Si ir function. The angle α is represented by Fig.5(*a*) d the r_{ij}(Si–Si) distance is related to α by

$$r_{ij}(\text{Si–Si})=2\times1{\cdot}62\sin\alpha/2\,.$$

o treat the broadening of the Si–Si peak it is best to e a distance distribution function $G(r_{ij},\text{Si–Si})$, but r the following peaks, Si–2nd O, O–2nd O, and -2nd Si it is more convenient to have an angular stribution function $V(\alpha)$. The distribution functions e related by

$$G(r_{ij})dr_{ij}=V(\alpha)d\alpha$$

nd since $dr_{ij}/d\alpha=1{\cdot}62\cos\alpha/2$

$$V(\alpha)=G(r_{ij})1{\cdot}62\cos\alpha/2\,. \qquad (8)$$

The two distribution functions $G(r_{ij})$ and $V(\alpha)$ which are shown by Fig.5(*b*) and (*c*) are related by equation 8), and chosen by trial to give the best agreement for he third, fourth and fifth peaks of Fig.4.

There is 1 Si in the unit of composition and each Si s expected to have 4 Si neighbors, so that for the third peak

$$\sum_{\text{uc}}\sum_{i} N_{ij}/r_{ij}=(1\times4)/3{\cdot}12\,.$$

The $G(r_{ij})$ of Fig.5(*b*) allows for a distance variation due to change in the angle α. In addition there is a variation due to change in the Si–O distance, and this was allowed for by another distance distribution function $G'(r'_{ij})$ which was taken proportional to 1·00 for $r'_{ij}=r_{ij}$, 1·00 for $r'_{ij}=r_{ij}\pm0{\cdot}05$, and 0·50 for $r'_{ij}=r_{ij}\pm0{\cdot}10$. The effective pair function was obtained from these two distance distributions by means of equation (7). Multiplying by 4/3·12 we obtain the Si–Si pair function distribution curve which is shown on Fig.4 at $r=3{\cdot}12$ Å.

The next peak occurs at about $r=4{\cdot}15$ Å. This is a Si–2nd O contribution, and the separation r_{ij}(Si–2nd O) which is shown by Fig.6(*a*), is given by

$$r_{ij}^2=9{\cdot}65-7{\cdot}00\cos\alpha-4{\cdot}96\sin\alpha\cos\beta\,. \qquad (9)$$

This time there are two angular variables, α and β. For α we have the distribution function $V(\alpha)$ of Fig.5(*c*), but there is no first hand information concerning the angle β. Since there are three oxygen atoms at 120° intervals on the circle of Fig.6(*a*), a variation in β of $\pm60°$ is equivalent to a variation from 0° to 360°. It is necessary to introduce various trial distributions for β and see which one gives the best agreement. The assumption that β takes with equal probability all values from 0° to 360° appeared to give satisfactory agreement. For all other assumptions which were tried, the agreement was definitely inferior.

The method used to compute $G(r_{ij})$ is illustrated by Fig.7. Values of r_{ij} are computed from equation (9) for a series of values of α and β. These are plotted on Fig.7 with a linear scale for β, and intervals proportional to $V(\alpha)$ for the variable α. Contours of constant r_{ij} are drawn, and the areas between contours measured with a planimeter. These areas are proportional to $G(r_{ij})$. In addition to this variation in distance due to α and β, there is also a variation due to changes in the Si–O distance. To allow for this we introduce a $G'(r'_{ij})$, which is taken constant for values of r'_{ij} between $r_{ij}-0{\cdot}10$ and $r_{ij}+0{\cdot}10$, and zero elsewhere. The effective pair function was then obtained by a double convolution. For this peak $\sum_{\text{uc}}\sum_{i} N_{ij}/r_{ij}=(1\times12+2\times6)/4{\cdot}15$. Multiplying the effective pair function by this factor gives the pair function distribution curve due to the Si–2nd O contribution. It is shown on Fig.4 by the dashed peak at about $r=4{\cdot}1$ Å.

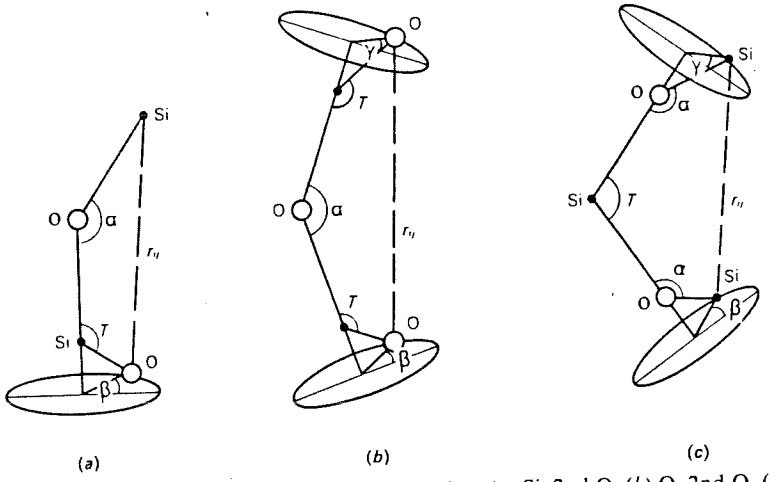

(*a*) (*b*) (*c*)

Fig.6. The relations between distances r_{ij} and the angular variables α, β, γ. (*a*) Si–2nd O. (*b*) O–2nd O. (*c*) Si–2nd Si. $T=109°28'$.

The fifth peak on Fig. 4 occurs at about $r = 5{\cdot}1$ Å, and this is a superposition of the two contributions O–2nd O and Si–2nd Si. The two distances r_{ij}(O–2nd O) and r_{ij}(Si–2nd Si) are shown by Fig. 6(*b*) and (*c*). To compute a $G(r_{ij})$, we assume that α follows the distribution $V(\alpha)$ of Fig. 5(*c*), and that β and γ independently take with equal probability all values from 0° to 360°. An additional variation as a result of change in the Si–O distance was represented by a $G'(r'_{ij})$ which was taken constant between $r'_{ij} = r_{ij} - 0{\cdot}10$ and $r'_{ij} = r_{ij} + 0{\cdot}10$ and zero elsewhere. The effective pair functions were then obtained by double convolutions. For O–2nd O

$$\sum_{\text{uc}} \sum_{i} N_{ij}/r_{ij} = 2 \times 18/5{\cdot}10 \ ;$$

For Si–2nd Si

$$\sum_{\text{uc}} \sum_{i} N_{ij}/r_{ij} = 1 \times 12/5{\cdot}10 \ .$$

Multiplying the effective pair functions by these two factors gave the pair function distribution curves due

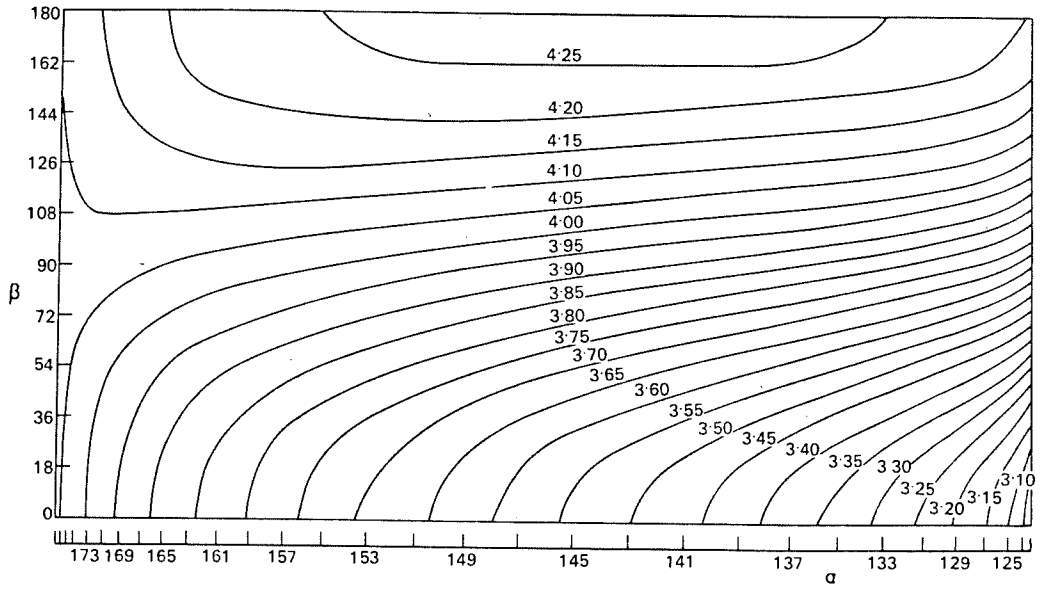

Fig. 7. Contours of constant r_{ij} for the Si–2nd O distance. The ordinate scale is linear in the angle β. For the abscissa scale α, the intervals are proportional to $V(\alpha)$.

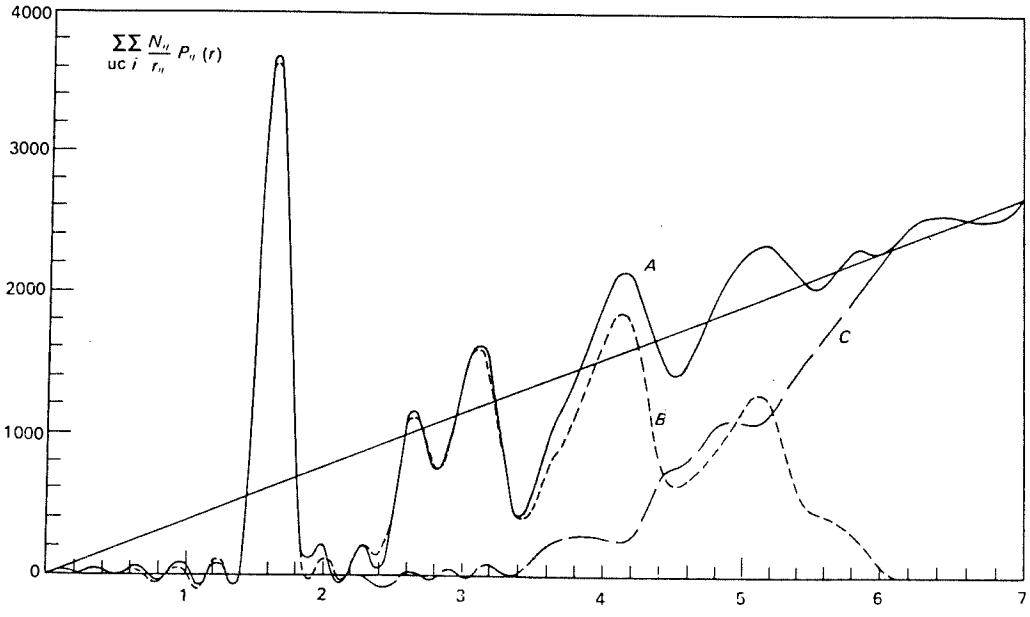

Fig. 8. The pair function distribution curve for SiO_2. *A* is the measured curve. *B* is the sum of the first six contributions: Si–O, O–O, Si–Si, Si–2nd O, O–2nd O, Si–2nd Si. *C* is the difference *A*–*B*.

to the O-2nd O and the Si–2nd Si contributions. The two peaks are shown by the dashed curves on Fig. 4 at about $r = 5{\cdot}1$ Å.

The computed peaks on Fig. 4 have all occurred at closely the positions of the peaks on the measured curve. To see how closely the areas are reproduced, it is necessary to take the sum of the computed contributions. For the first six pairs: Si–O, O–O, Si–Si, Si–2nd O, O–2nd O, and Si–2nd Si, the sum is shown on Fig. 8, curve *B*, along with the measured pair function distribution curve, *A*. The agreement is very satisfactory through the third peak, but beyond $r = 3{\cdot}4$ Å there is a difference which is not predicted by the first six contributions. It is doubtful if the fluctuations in the rising part of the difference curve have much significance, since they would be greatly changed by small variations in the calculated contributions. The difference curve, *C*, rises to a maximum at about $r = 6{\cdot}4$ Å. This is the last peak in the measured distribution curve, beyond $r = 7{\cdot}0$ Å there are no further peaks and dips.

A large part of the difference curve and the maximum at $r = 6{\cdot}4$ Å are probably due to the Si–3rd O contribution. Since we have been assuming a random network in which there is complete randomness in orientation about each Si–O bond, it seems at first sight unlikely that the Si–3rdO contribution could produce an observable peak. However, the fact that the most probable value of α is around 144° leads to a geometrical relation which suggests that a peak in the Si–3rd O contribution at around 6·4 Å is at least possible. With 144° as the most probable value of α, the geometrical relation is shown by Fig. 9. The Si(1) atom takes with equal probability all positions on the upper left hand circle. The O(3) atom takes all orientations about the O(2)–Si(3) bond, giving a high oxygen density on the circle O(3)–*A*. But since the O(2)–Si(3) bond takes all orientations about the Si(2)–O(2) direction, the circle O(3)–*A* takes all orientations about the Si(2)–O(2) direction, and this results in a high oxygen density in the vicinity of position *A*. Independent of the orientation of the O(1)–Si(2) bond around the Si(2)–O(2) direction, the distance *l*[Si(1)–*A*] is given by

$$l^2 = 35{\cdot}77 + 7{\cdot}60 \cos\beta\,.$$

The values of β in the range between $\pm 90°$ give a $G(r_{ij})$ for Si(1)–*A*, which when convoluted with the Si–O pair function, produces a peak at about $r = 6{\cdot}4$ Å. This seems to be the last peak which could be produced in the random type of network which we have been considering, and in fact no further peaks are observed on the measured pair function distribution curve.

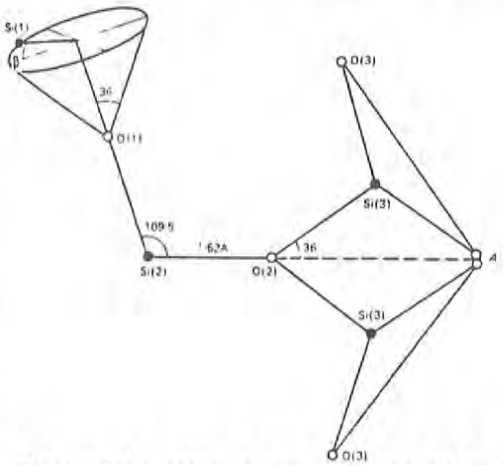

Fig. 9. The special geometry which applies to the Si–3rd O distance, using for the Si–O–Si angle the most probable value $\alpha = 144°$.

Discussion

It should be emphasized that a measured pair function distribution curve such as that of Fig. 4 represents a structure which is averaged over the whole sample. If in a few small regions there is a higher degree of order such as that of the cristobalite and quartz structures, this could not be recognized as such, and the contributions of these regions would show up only as part of the general average. An X-ray study of a sample of low cristobalite gave a pair function distribution curve which was very similar to that of vitreous silica for the first two peaks, but appreciably narrower for the third peak. Beyond the third peak the differences became progressively greater, and whereas the vitreous silica curve showed no detail beyond about $r = 7{\cdot}0$ Å, the cristobalite curve continued to show strong peaks and dips out to the largest value ($r = 12$ Å) to which the curve was evaluated.

In recent years there has been considerable interest in studying the random network model of vitreous silica by making a model out of tetrahedral units joined in a random fashion (Ordway, 1964; Evans & King, 1966; Bell & Dean, 1966). From such a model it is possible to tabulate average numbers of neighbors and distances. With the data of Evans & King, which were kindly supplied by Dr Evans, a histogram was constructed and found to be in very satisfactory agreement with the measured curve of Fig. 4.

From the pair function distribution curve it is possible to draw a number of definite conclusions about the structure of vitreous silica. Practically all of the silicon atoms are tetrahedrally bonded to 4 oxygen atoms, with an average Si–O distance of 1·62 Å. Practically all of the oxygen atoms are bonded to 2 silicon atoms. The Si–O–Si bond angle α follows the distribution curve $V(\alpha)$, and it varies all the way from 120° to 180° with a maximum at about $\alpha = 144°$. This wide variation in the Si–O–Si bond angle is the first distinction between the vitreous and the crystalline forms of silica, and it is a very important criterion for any proposed model of vitreous silica. On the average there appears to be a random orientation about the Si–O bond directions, except where prevented by the close approach of neighbors. The only justification for this conclusion comes from the fact that pair function cal-

culations were in better agreement for random orientations than for any of the special orientations which suggested themselves. It would be of great interest to know the fraction of five, six and seven membered rings in the structure, but unfortunately it does not appear possible to get this information directly from the X-ray results. The structure which has developed in this analysis is, of course, that of the familiar random network, but with the new results we can now give a much more precise description of the structure.

This work was done in part at the Computation Center at the Massachusetts Institute of Technology, Cambridge. One of us (RLM) was a Raytheon Graduate Program Member at M.I.T.

References

BELL, R. J. & DEAN, P. (1966). *Nature, Lond.* **212**, 1354.
CARRARO, G. & DOMENICI, M. (1963). *Vetro e silicati*, **7**, 6.
CROMER, T.D. (1965). *Acta Cryst.* **18**, 17.
CROMER, D. T. & WABER, J. T. (1965). *Acta Cryst.* **18**, 104.
EVANS, D. L. & KING, S. V. (1966). *Nature, Lond.* **212**, 1353.
HENNINGER, E. H., BUSCHERT, R. C. & HEATON, L. (1967). *J. Phys. Chem. Solids.* **28**, 423.
International Tables for X-ray Crystallography (1962). Vol. III. Birmingham: Kynoch Press.
NORMAN, N. (1957). *Acta Cryst.* **10**, 370.
ORDWAY, F. (1964). *Science*, **143**, 800.
VALENKOV, N. & PORAI-KOSHITZ, E. (1936). *Z. Kristallogr.* **95**, 195.
WARREN, B. E., KRUTTER, H. & MORNINGSTAR, O. (1936). *J. Amer. Ceram. Soc.* **19**, 202.
WARREN, B. E. & MAVEL, G. (1965). *Rev. Sci. Instrum.* **36**, 196.
WARREN, B. E. & MOZZI, R. L. (1966). *Acta Cryst.* **21**, 459.
WARREN, B. E. (1969). *X-ray Diffraction*, pp. 135–142. Reading: Addison–Wesley.
ZARZYCKI, J. (1957). *Verres et Refractaires*, **1**, 3.

J. Appl. Cryst. (1969). **2**, 172

Measurement of X-ray Orientation Factor in Cellulose II Fibres

BY V. VENKATAKRISHNAN

The South India Textile Research Association, Coimbatore-14, India

(*Received* 16 *May* 1969)

For the measurement of crystallite orientation in regenerated cellulosic fibers, Hermans and co-workers defined a parameter K in terms of the intensity distribution in the (10$\bar{1}$, 021) sickle. Their theory is extended in the present study to mercerized fibers. It is found from the experimental observations that *K is itself dependent on the X-ray orientation factor*, and possible reasons for this are advanced. The dependence of K on the ratio of the number and diffractive powers of (021) and (10$\bar{1}$) planes is, however, confirmed. A regression equation based on the correlation of K with the readily observed relative peak height of 021 is found to be of practical interest in estimating the crystallite orientation.

Symbols used

f_x X-ray orientation factor.

B diatropic interference arising from the planes (020).

β inclination of the fiber axis to the crystallographic b axis.

$J(\beta)$ intensity distribution in the arc of B.

A_0, A_3 and A_4 interferences arising from X-ray scattering by the paratropic planes (101), (10$\bar{1}$) and (002) respectively.

α_0, α_3, and α_4 azimuthal angles along the arcs A_0, A_3 and A_4 respectively, measured from the equator.

$F(\alpha)$ intensity distribution in the paratropic reflexions in general.

F_0, F_3, F_4 intensity distributions in the paratropic reflexions A_0, A_3 and A_4 respectively.

t azimuthal angle along the arc due to the unresolved reflexions from (10$\bar{1}$) and (021) planes.

γ azimuthal angle of the resolved part of the curve due to reflexion 021.

$F(\gamma)$ intensity distribution in the resolved reflexion (021).

Introduction

All fibrous materials exhibit a preferred orientation varying only in degree. The extent of preferred orientation has an important bearing on many physical characteristics of these materials, especially their tensile behaviour. Hermans, Hermans, Vermaas & Weidinger (1946) have done extensive work on the technique of measuring orientation both in cellulose I (native cotton,